Journal of Power Sources 196 (2011) 7564–7571

Contents lists available at ScienceDirect

Journal of Power Sources

journal homepage: www.elsevier.com/locate/jpowsour

The performance of a novel pseudo-bipolar bi-cell piezoelectric proton exchange membrane fuel cell with a smaller nozzle and diffuser

Hsiao-Kang Ma*, Jyun-Sheng Wang, Wei-Han Su, Wei-Yang Cheng

Department of Mechanical Engineering, National Taiwan University, Taipei 10617, Taiwan

ARTICLE INFO

Article history:
Received 24 February 2011
Received in revised form 14 April 2011
Accepted 14 April 2011
Available online 21 April 2011

Keywords:
Piezoelectric
Diffuser
Pseudo-bipolar
Bi-cell
Fuel cell
Performance

ABSTRACT

Previous studies of a bi-cell piezoelectric proton exchange membrane fuel cell with a nozzle and diffuser (PZT-PEMFC-ND bi-cell), using a novel pseudo-bipolar design, have shown that the performance of the bi-cell could be 1.6 times greater than that of the single cell. In this study, this novel design, using a reduced nozzle and diffuser, contains two cells with two outside anodes and two inside cathodes that share a common PZT vibrating device for pumping air flow. The results show that the bi-cell should be operated with a larger stoichiometric ratio of 1.5 and a cell temperature of 50 °C to prevent concentration loss. Furthermore, the performance of the bi-cell using one degraded membrane electrode assembly (MEA) and one normal MEA is investigated to understand the current flow characteristic of the bi-cell. Although an internal current is observed, the bi-cell can still deliver a non-negative power. This finding will help reinforce the viability of using a PZT-PEMFC-ND bi-cell for future stack designs. Moreover, the power consumption of the PZT device is temperature-dependant and this should be taken into consideration when determining the net power of the PZT-PEMFC-ND bi-cell. The maximum net power of the bi-cell is found to be 0.7 W.

1. Introduction

Over the past several years, the proton exchange membrane fuel cell (PEMFC) has been an attractive option in the renewable energy industry due to its adaptability to a variety of applications and its zero emissions capabilities [1–3]. For portable PEMFC application, the air-breathing concept is usually adopted to reduce the auxiliary oxygen supply system, such as compressors and humidifiers, to support PEMFC performance. In these cases, the air supply device should be small, provide sufficient air flow, and require low power consumption. Various actuating methods, such as electrostatic, magnetostriction, shape memory alloy, thermopneumatic, and piezoelectric actuators, have been developed to pump fluid in a precise manner. Among these actuating methods, the piezoelectric actuator demonstrates good reliability, energy efficiency, and moderate volume displacement [4]. To improve its pumping flow rate, Olsson [5], Ullmann [6], and Yang [7] have investigated the piezoelectric valveless micropump system in which two chambers are placed in a series or in a parallel arrangement. The results show that the flow rate in a piezoelectric actuator could be controlled by changing the phase difference.

During operation of an AB-PEMFC, membrane hydration plays an important role in proton conductivity, which determines the efficiency of the electrochemical reaction. Furthermore, the hydration is affected by the conditions of the inlet gases and by the cell temperature [8,9]. Operating parameters that facilitated better water removal by evaporation, such as higher temperature, stoichiometric flow rates, and lower inlet stream humidity, resulted in a higher net current. Yi and Nguyen [10] showed that PEMFC performance was improved by anode humidification and by positive differential pressure between the cathode and anode, factors that are also proved by the Nernst equation. Lower cell temperature, and, hence, higher water condensation in the anode channels, may contribute to anode flooding [11]. A larger stoichiometric ratio is often used to mitigate the flooding. However, this might result in the membrane drying out because the gas might cause too much water to escape into the outlet.

In previous studies, many simulation models have been developed to understand complex transport and electrochemical phenomena in PEMFCs, such as open-circuit voltage, ohmic resistance, and polarization losses. Almost all the models proposed for the PEMFC consist of mathematical equations and are not very useful in power converter and system simulations [12]. In order to simulate the fuel cell behavior effectively, especially in steady-state conditions, several equivalent circuit models are developed

* Corresponding author at: Department of Mechanical Engineering, National Taiwan University, No. 1, Roosevelt Road, Section 4, Taipei 10617, Taiwan.
Tel.: +886 2 23629976; fax: +886 2 23632644.
E-mail address: skma@ntu.edu.tw (H.-K. Ma).

0378-7753/$ – see front matter © 2011 Elsevier B.V. All rights reserved.
doi:10.1016/j.jpowsour.2011.04.027

Nomenclature

A	cross-section area
A_{PZT}	piezoelectric area (m^2)
AR	aspect ratio
C	conductivity coefficient
D	channel opening width
f	frequency of PZT (Hz)
L	channel path
P	pressure ($N\,m^{-2}$)
P_c	channel pressure
P_{in}	inlet pressure
P_{out}	outlet pressure
R	gas constant ($J\,mol^{-1}\,K^{-1}$)
R_Ω	ohmic resistance
R_{ct}	charge transfer resistance
t	time (s)
T	temperature (K)
T_{an}	anode inlet temperature
V	open-circuit voltage of a bi-cell
V_c	cathode inlet velocity ($m\,s^{-1}$)
V_{PZT}	motion equation of the piezoelectric device ($m\,s^{-1}$)
Q	flow rate
Q_{An}	anode flow rate
Z_i	internal resistance
Z_W	finite-length Warburg impedance
Λ	amplitude
ζ	loss coefficient
θ	diffuser angle
ρ	density ($kg\,m^{-3}$)
$\forall$	volume displacement (m^3)

[13–15]. These circuit models usually consist of an inductor, a resistor in the high frequency region, and two parallel RC circuits connected in a series. The inductor accounts for the influence associated with the external electrical connections. The resistor responds to the activation resistance, the ohmic resistance, and the concentration transfer resistances. The parallel RC elements simulate the kinetic and mass transport behaviors. In the RC circuit, the capacitor is modeled as a constant phase element to account for the capacitive losses that generally occur in the porous electrode [15]. However, these models are developed for stacks using a bipolar design. Few models are proposed to analyze the monopolar design and the pseudo-bipolar design [16], especially those with degraded components, such as a membrane electrode assembly (MEA). Degraded MEAs would burden the performance due to the larger resistance and the lower voltage that results from gas crossover and contamination [17].

Previous studies [18–21] of a novel piezoelectric proton exchange membrane fuel cell with a nozzle and diffuser (PZT-PEMFC-ND) have shown that a PZT device could solve these flooding problems and improve cell performance. The piezoelectric device is an actuator that pumps air into the cathode chamber, delivering a better performance and a higher current generation. The results also showed that improved PZT-PEMFC-ND cell performance could be obtained using the appropriate aspect ratio (AR) of the diffuser elements in order to prevent the blocking phenomenon. Furthermore, a bi-cell piezoelectric proton exchange membrane fuel cell with nozzle and diffuser (PZT-PEMFC-ND bi-cell) has been developed and its performance could be 1.6 times greater than that of a single cell [22].

The objective of this study is to investigate the performance of a PZT-PEMFC-ND bi-cell with a reduced diffuser design using a novel pseudo-bipolar design under various operating conditions,

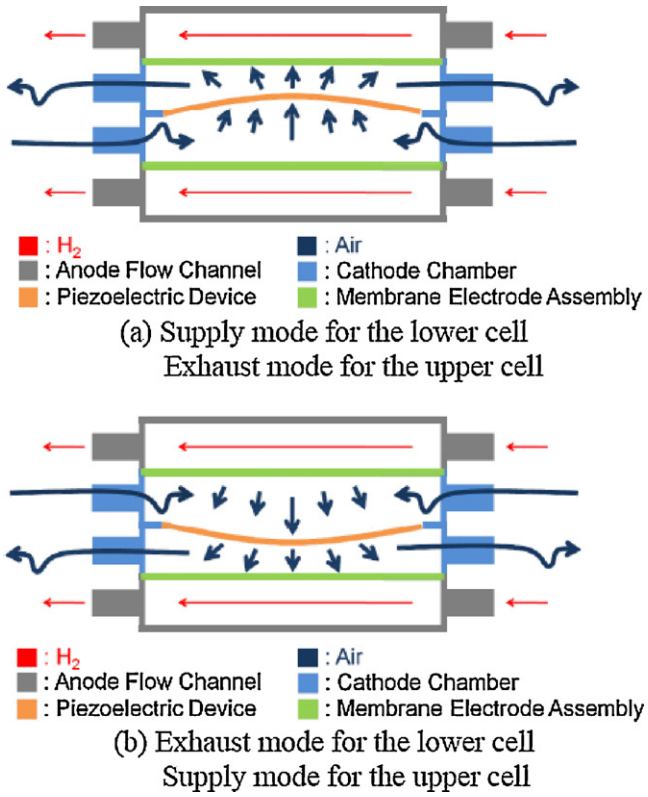

Fig. 1. Operation modes of the PZT-PEMFC-ND bi-cell.

including different cell temperatures and varying stoichiometric ratios. Moreover, these parameters are applied to a bi-cell using a degraded MEA and a normal MEA to better understand the operating characteristics of the bi-cell. Furthermore, to optimize the integrated system output, the net power of the bi-cell and the power consumption of the PZT device are taken into consideration.

2. The novel pseudo-bipolar design of the air-breathing PZT-PEMFC-ND

2.1. The concept of the novel pseudo-bipolar design

Various PEMFC stacks have been developed based on different considerations of functional demands and system designs [23]. The traditional pseudo-bipolar design contains two cells with two inside anodes and two outside cathodes. Typically, the PEMFC stack is constructed using the bipolar design. However, because two piezoelectric devices are required for a PZT-PEMFC-ND bi-cell, using the bipolar design may decrease the net power output of the bi-cell. Thus, the PZT-PEMFC-ND bi-cell was constructed using the novel pseudo-bipolar design to deliver increased power. As shown in Fig. 1, this innovative design differs from the traditional design, which consists of two cells with two outside anodes and two inside cathodes that share a common PZT vibrating device used to pump air flow. This novel arrangement allows one PZT device to supply air to the two component cells and pump the produced water out of the cells, reducing power consumption.

2.2. The circuit model of a bi-cell

The PZT-PEMFC-ND bi-cell, using the novel pseudo-bipolar design, can be depicted with modified Randles-Ershler circuits and ideal potential sources, as shown in Fig. 2. R_Ω, R_{ct}, and Z_W represent ohmic resistance, charge transfer resistance, and finite-length

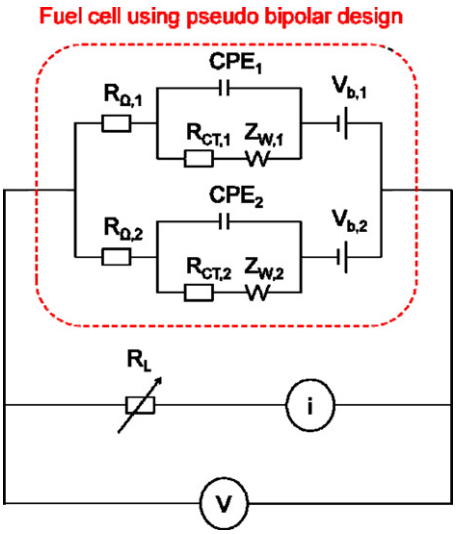

Fig. 2. The equivalent circuit model of the PZT-PEMFC-ND bi-cell.

Warburg impedance, respectively [24]. The conventional double layer capacitance is replaced by a constant phase element (CPE) to account for non-uniform diffusion. The internal resistance Z_i of the component cell could be stated as the sum of the impedance of these components. Thus, the open-circuit voltage of the bi-cell could be written using Kirchhoff's circuit laws, as follows:

$$V = \left[\frac{Z_{i,2}}{Z_{i,1}+Z_{i,2}}\right] \times V_{b,1} + \left[\frac{Z_{i,1}}{Z_{i,1}+Z_{i,2}}\right] \times V_{b,2} \quad (1)$$

2.3. Actuation mechanism

In a PZT-PEMFC-ND bi-cell, two diffuser elements are applied to induce a larger air flow rate, as shown in Fig. 3. The geometrical parameters of the diffuser, including the diffuser angle (θ) and the aspect ratio (AR), affect pump performance. The lumped system, developed by Ullmann [6], was applied to analyze the characteristics of the valveless PZT pumping system. This method neglected spatial variations and, instead, focused on time variations that do not require complex CFD methods, such as the Navier–Stokes equations. As shown in Fig. 4, the time variation method was conducted for the following: exhaust mode ($P_c > P_{out} > P_{in}$), supply mode ($P_{out} > P_{in} > P_c$), and transition mode ($P_{out} > P_c > P_{in}$). An assumption was made that the inlet pressure, P_{in}, was always smaller than the outlet pressure, P_{out}, due to the nozzle/diffuser design. In the supply mode, the diaphragm moved outward and the cathode chamber volume increased, which caused the chamber pressure to be lower than the atmospheric pressure. Thus, the air was sucked into the chamber. In the exhaust mode, the diaphragm moved

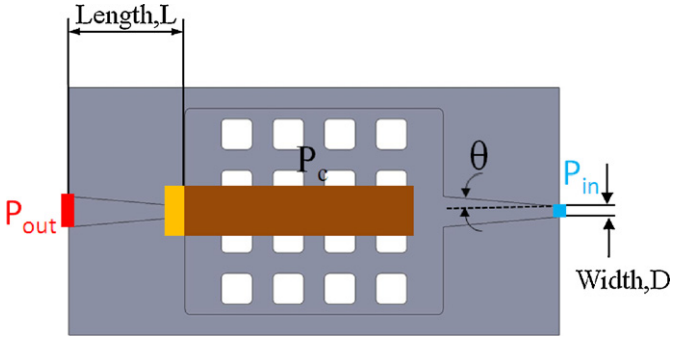

Fig. 3. The cathode chamber design of the PZT-PEMFC-ND bi-cell.

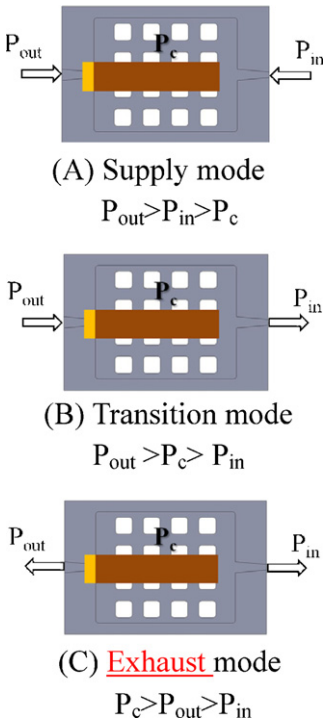

Fig. 4. The flow modes during the pumping process.

inward and the cathode chamber volume decreased. Because the pressure inside the cell was higher than the atmospheric pressure, the air was pushed into the catalyst layer and the resulting water was pumped out of the cell. Between the exhaust mode and the supply mode, a transition mode occurred when the outlet pressure was higher than the chamber and inlet pressures, $P_{out} > P_c > P_{in}$.

To analyze the air flow rate of the PZT-PEMFC-ND system, the system's control volume was chosen in the cathode chamber. The equation of motion for the PZT device was a sine function given by Eq. (2).

$$\vec{V}_{PZT} = \frac{d}{dt}[-\Lambda \times (\sin(2\pi f t))]. \quad (2)$$

Thus, by using the Reynolds Transport Theorem and the continuity equation [18–21], the air flow rate can be written as:

$$Q_c = \frac{1}{R}\frac{\partial}{\partial t}\int_{CV}\frac{P}{T}d\forall + \rho\vec{V}_{PZT}A_{PZT}. \quad (3)$$

The inlet flow from the nozzle and diffuser could be found by using the diffuser element theory and the continuity equation, as follows:

$$Q_{in,l} = C_n\sqrt{(P_{out} - P_C)} \quad \text{for the air inflow from left to right} \quad (4)$$

$$Q_{in,r} = C_d\sqrt{(P_{in} - P_C)} \quad \text{for the air inflow from right to left} \quad (5)$$

where the conductivity coefficient can be separated into nozzle, C_n, and diffuser, C_d.

$$C_n = \frac{A}{\sqrt{(1/2)\xi_n\rho}} \quad (6)$$

$$C_d = \frac{A}{\sqrt{(1/2)\xi_d\rho}} \quad (7)$$

Thus, the inlet flow rate is given by Eq. (8), as follows:

$$Q_{in} = Q_{in,l} + Q_{in,r} \quad (8)$$

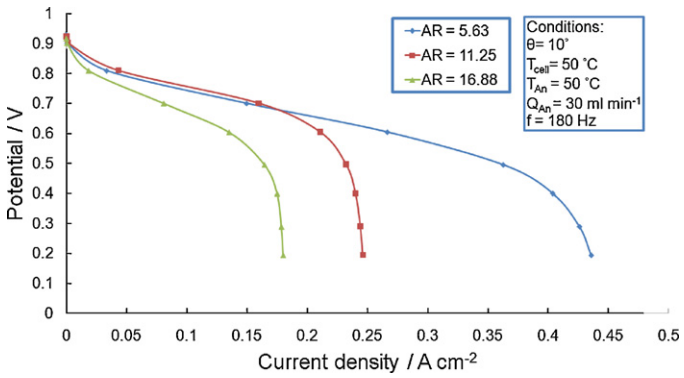

Fig. 5. The *I–V* curves under different aspect ratios at $T_{cell} = 50\,^{\circ}C$, $T_{An} = 50\,^{\circ}C$, $f = 180$ Hz and $\theta = 10^{\circ}$.

2.4. The improved diffuser design

A previous study [22] showed that PZT-PEMFC-ND module performance would be restricted by the blocking phenomenon induced by a larger aspect ratio. As such, the better geometrical parameters are an AR of 11.25 and a θ of 5°. The aspect ratio is defined as the channel length divided by the channel opening width. The channel opening width is 1 mm, so the channel length is 11.25 mm. In order to reduce the size of the bi-cell, a smaller aspect ratio is required. Thus, the performance of the PZT-PEMFC-ND is investigated with a larger θ of 10° and different ARs, as shown in Fig. 5. The results showed that the performance improves when a smaller AR of 5.63 is used. Thus, the channel length is reduced to 5.63 mm. A three-dimensional transitional model, based on the semi-implicit method for pressure line equations consistent (SIMPLEC) procedure, was used to analyze the effects of the diffuser geometry on the flow behavior of the PZT-PEMFC-ND, as described in [22]. As shown in Fig. 6, the velocity profiles in the supply mode reveal that the blocking phenomena occurred in cases with an AR of 11.25 and 16.88. Thus, a better performance is obtained when the size of the bi-cell is smaller and when a smaller AR of 5.63 and a larger θ of 10° are used.

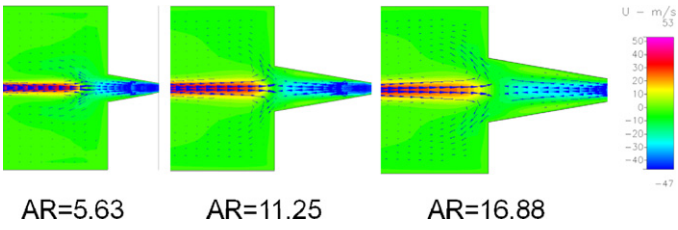

Fig. 6. Velocity profiles under different aspect ratios at $\theta = 10^{\circ}$.

3. Experimental setup

Fig. 7 shows the test platform used to analyze PZT-PEMFC-ND bi-cell performance. On the anode side, the hydrogen from the hydrogen storage bottle flowed through the mass flow controller and entered the bubble humidifier. The humidifier was a water tank with a heater that allowed the reactant gas to pass through at a specific temperature. Next, the hydrogen with water vapor was delivered to the PZT-PEMFC-ND module for an electrochemical reaction. The equipment on the cathode side was more complex than the equipment on the anode side. To activate the PZT vibrating device, a function generator was utilized to first deliver the sine wave signals. The signals from the function generator were then sent to an amplifier to magnify the signals, so that the piezoelectric device vibrated when it received the signal. To measure the power

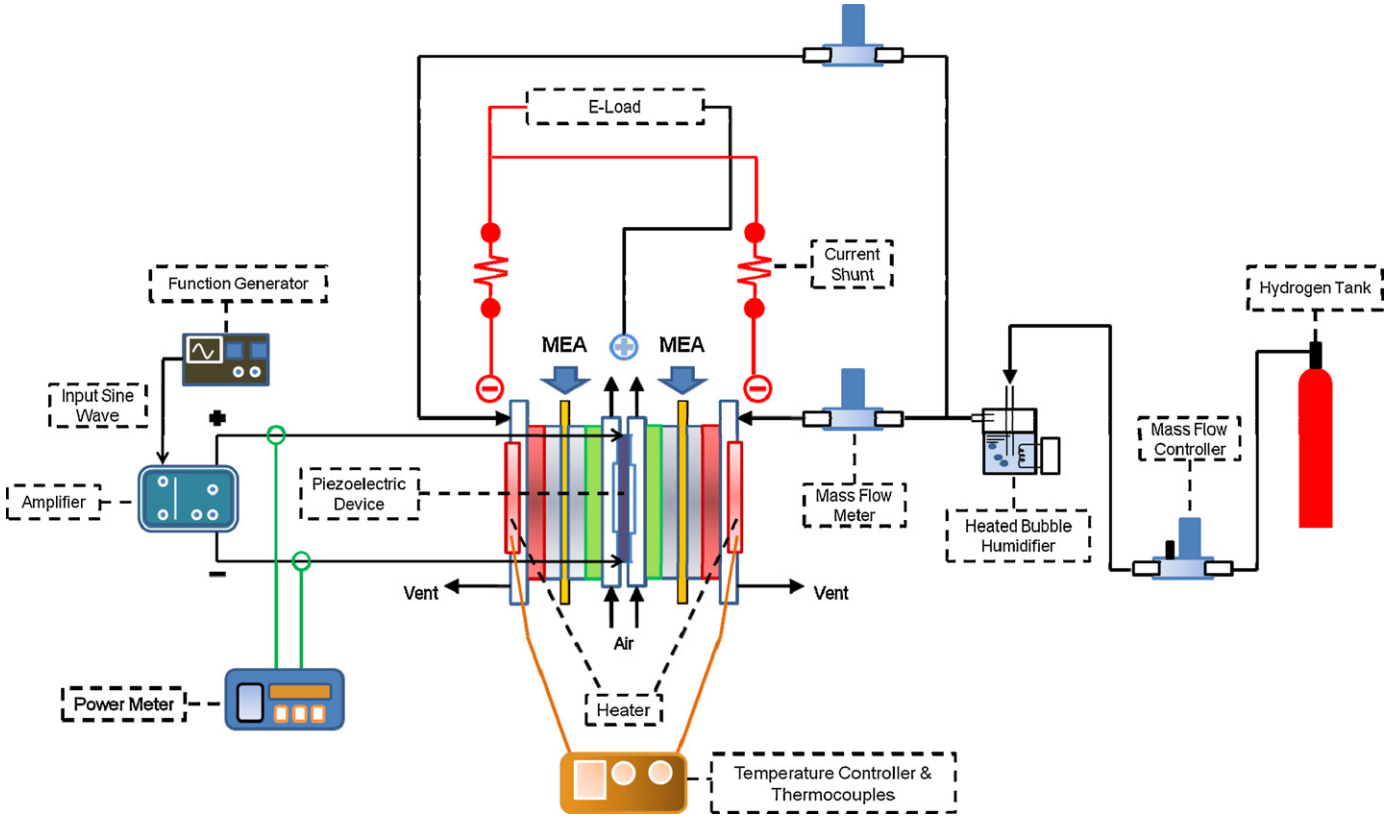

Fig. 7. Schematic of the PZT-PEMFC-ND bi-cell testing system.

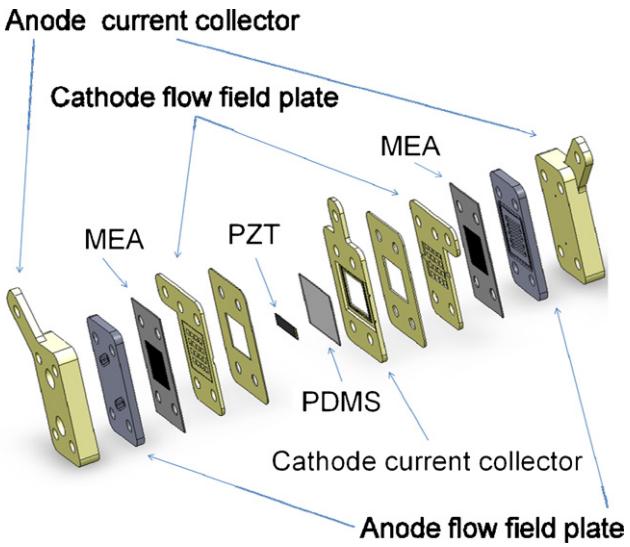

Fig. 8. An exploded drawing of the PZT-PEMFC-ND bi-cell.

consumption of the PZT device, a power meter was connected to the output terminals of the amplifier.

The PZT-PEMFC-ND bi-cell, shown in Fig. 8, consists of two anode current collectors, two anode flow field plates, two MEAs, one PZT device, and one cathode current collector. The reaction area of the MEA is $2 \times 2\,cm^2$, the membrane is Nafion®212, and the opening ratio is 34.7% in the cathode. To prevent gas leakage, the PZT material (BM 70/25/200M, Piezomechanik GmbH) is attached to a gasket film, made of PDMS, on the cathode current collector. Fig. 9 shows the assembled bi-cell and the setup of the bi-cell experiment. In this study, the two cells were electrically parallel. Thus, two hydrogen supply lines and two thermocouples were prepared. In contrast, the signal from the amplifier was transmitted through the signal wires in the middle of the module.

The PZT device of the PZT-PEMFC-ND bi-cell was driven by a sine wave signal generated by a function generator. The amplifier was required to magnify voltage to the designated dB. The vibration frequency of the PZT device was set at 60 Hz because a frequency that is too large unfavorably affects the lifetime of the PZT material. Thus, the PZT device controlled the air flow on the cathode side. The ambient condition was considered to be an environmental temperature of 22 °C and a relative humidity of 60%. The amplitude of the PZT device was measured using a laser displacement measurement sensor (AR200-6M, Acuity). The hydrogen in the anode side was supplied by hydrogen storage and controlled by the mass flow controller. Next, two flow meters were prepared to monitor the flow rate into the different component cells. The DC electronic load simulated the electronic loading of voltage and current. In this study,

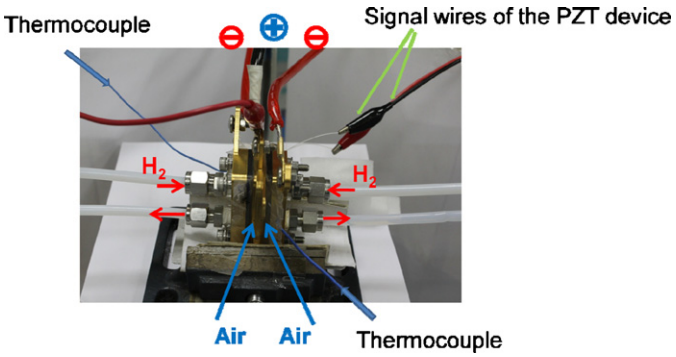

Fig. 9. Experimental setup of the PZT-PEMFC-ND bi-cell.

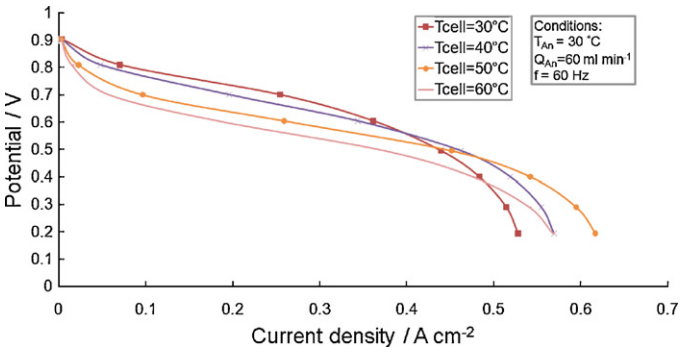

Fig. 10. The *I–V* curves under different cell temperatures at $T_{An} = 30\,^{\circ}C$, $Q_{An} = 60\,ml\,min^{-1}$, and $f = 60\,Hz$.

a constant voltage mode was chosen and the polarization curves were obtained by decreasing 0.1 V from an open-circuit voltage to 0.2 V every 10 min, using LabVIEW software. Furthermore, two current shunts were prepared to measure the currents through each of the cells.

4. Results and discussion

In this study, the influence of the cell temperature and the stoichiometric ratio (λ), at a 10° diffuser angle and a reduced aspect ratio of 5.63, were investigated to determine the performance of the PZT-PEMFC-ND bi-cell. The bi-cell performance was then considered with regard to the power consumption of a PZT device in order to estimate the net power of the PZT-PEMFC-ND bi-cell. The better parameters were applied to a bi-cell using a degraded MEA to understand the current flow characteristics of the bi-cell.

4.1. Influence of the cell temperature

The performance of the AB-PEMFC with a traditional pseudo-bipolar design was affected by the humidity in the surrounding environment and by the operational temperature [25]. In this study, the cell temperature changes from 30 °C to 60 °C while maintaining the temperature of the humidified anode inlet gas at 30 °C. Fig. 10 shows the *I–V* curves under different cell temperatures at $T_{An} = 30\,^{\circ}C$, $Q_{An} = 60\,ml\,min^{-1}$, and $f = 60\,Hz$. As the cell temperature increases from 30 °C to 50 °C, the current output and cell performance increase because a high cell temperature improves the chemical reaction rate and induces a lower anode humidified condition that facilitates water removal. However, the bi-cell performance does not increase significantly with increasing temperature. This may be due to the fact that lower anode relative humidity also induces a larger back diffusion of water which is unfavorable for the electron transfer. Additionally, the current density and the cell performance decrease as the cell temperature increases from 50 °C to 60 °C because a larger activation loss was induced. Thus, the bi-cell should be operated under a cell temperature of 50 °C. This condition is favorable for reducing the humidification system loading in future applications of a portable PZT-PEMFC-ND stack.

4.2. Influence of the PZT amplitude

In this study, the component cell currents were monitored simultaneously using two current shunts to analyze PZT-PEMFC-ND bi-cell performance. Fig. 11 shows the *I–V* curves of the bi-cell and the component cells at $T_{cell} = 50\,^{\circ}C$, $T_{An} = 30\,^{\circ}C$, $Q_{An} = 60\,ml\,min^{-1}$, and $f = 60\,Hz$. The test results revealed that these two MEAs performed differently under the same cell temperature,

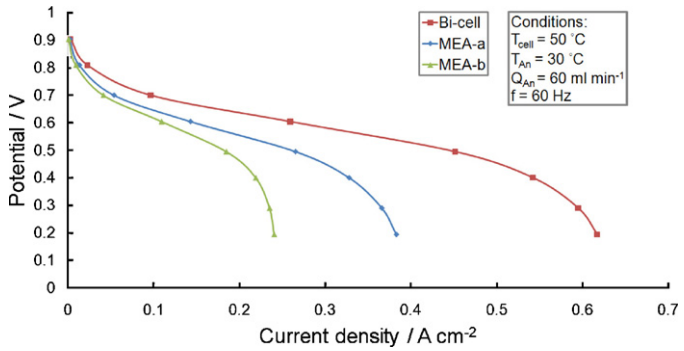

Fig. 11. The *I–V* curves of the bi-cell and the component cells at T_{cell} = 50 °C, T_{An} = 30 °C, Q_{An} = 60 ml min^{-1}, and f = 60 Hz.

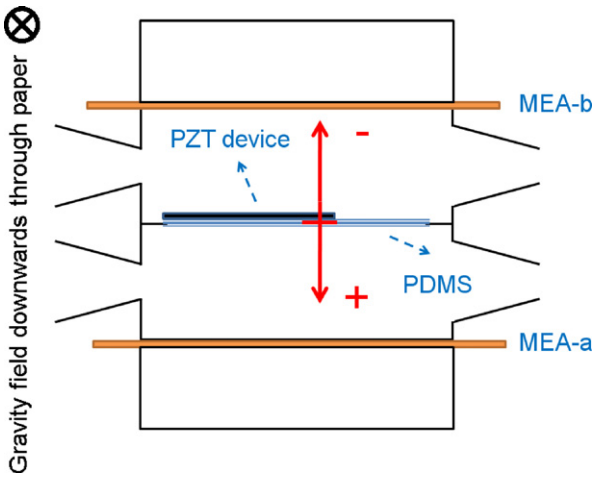

Fig. 12. The coordinates of the PZT device vibration.

the same hydrogen flow rate, and the same anode inlet temperature. Why was this so? Since the air flow to the cathode was driven by the PZT vibrations, the amplitude of the PZT device was the key element affecting the performance. The PZT material was attached to one side of the film made of PDMS. The origin of vibration was set at the tip of the PZT material. The positions of the MEAs are shown in Fig. 12. The positive amplitude is the amplitude toward MEA-a, and the negative amplitude is the amplitude toward MEA-b. Obviously, the negative amplitude is closer to MEA-b and causes the smaller cathode chamber volume of MEA-b.

Fig. 13 shows an amplitude variation ranging from 0.10 mm to −0.14 mm. Furthermore, the amplitude for the supply mode and the exhaust mode is not the same in each of the component cells. Eqs. (2)–(5) show that the inlet flow rate is decided by the amplitude. Since the negative amplitude is larger than the positive

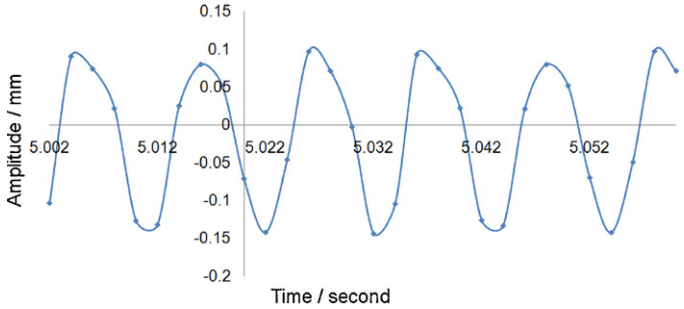

Fig. 13. The amplitude of the PZT device.

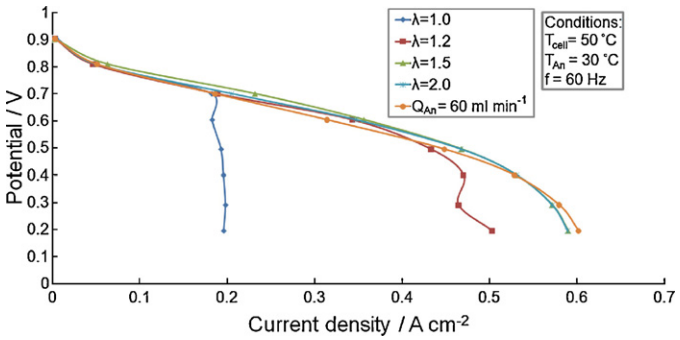

Fig. 14. The *I–V* curves under different stoichiometric ratios at T_{cell} = 50 °C, T_{An} = 30 °C, and f = 60 Hz.

amplitude, the supply mode in MEA-a may suck more air than the supply mode in MEA-b and, thus, MEA-a generates more current. Therefore, asymmetric amplitude might influence the performance of the component cells in the bi-cell and, thus, the performance of the bi-cell is not double that of a single cell.

4.3. Influence of the stoichiometric ratio

A stoichiometric ratio (λ) is often applied as a design guide to achieve a higher current output. If λ is too large, the membrane might dry out and the fuel efficiency might be reduced. In portable applications of PEMFC, low fuel efficiency is unfavorable.

The influence of the stoichiometric ratio on the performance of the PZT-PEMFC-ND bi-cell is shown in Fig. 14. The results show that the performance of the bi-cell increases when λ increases from 1 to 1.5 and the concentration loss is alleviated. However, operating the bi-cell with a λ larger than 1.5, or a constant anode hydrogen flow rate of 60 ml min^{-1}, would not improve its performance. Thus, a stoichiometric ratio of 1.5 was chosen as the optimal parameter for the PZT-PEMFC-ND bi-cell under T_{An} = 30 °C, T_{cell} = 50 °C, and f = 60 Hz.

Furthermore, serious concentration loss occurred when the λ was smaller. As shown in Fig. 15, the MEA-b performance is worse than the MEA-a performance in the concentration loss region at λ = 1.2. However, while the same hydrogen flow rates are supplied to both component cells, insufficient hydrogen is supplied to generate current in MEA-a, which may lead to a heavier flooding phenomenon.

4.4. Influence of the degraded MEA in the bi-cell

The degraded MEA was prepared by stripping the hot-pressed gas diffusion electrodes from the membrane and then re-attaching them to the membrane. This procedure resulted in a degraded MEA

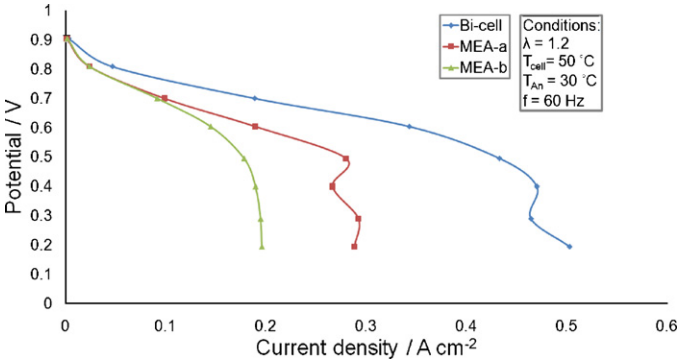

Fig. 15. The *I–V* curves of the bi-cell and the component cells at λ = 1.2, T_{cell} = 50 °C, T_{An} = 30 °C, and f = 60 Hz.

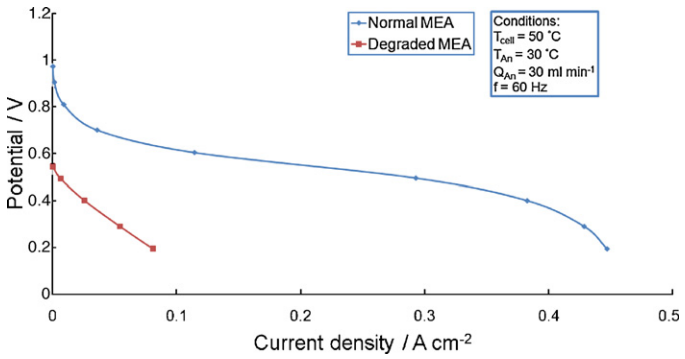

Fig. 16. Normal MEA and degraded MEA performance.

performance that was significantly lower than the normal MEA performance. The open-circuit voltage was 0.54 V, as shown in Fig. 16. Next, the bi-cell was assembled using a normal MEA and a degraded MEA, which were placed in the positions of MEA-a and MEA-b, respectively.

Fig. 17 shows the performance of the bi-cell and the component cells operated with a degraded MEA under T_{cell} = 50 °C, T_{An} = 30 °C, Q_{An} = 60 ml min^{-1}, and f = 60 Hz. The open-circuit voltage drops from 0.9 V to 0.84 V and, from Eq. (1), it can be seen that the impedance of the degraded MEA may be ten times larger than the impedance of the normal MEA. Because the bi-cell is electrically parallel, its current output results from the component cell and the current generated from the degraded MEA is negative at open-circuit voltage, which means an internal current exists inside the bi-cell. This internal current may result from the voltage difference between the component cells. The degraded MEA contributes to the performance from an operating voltage lower than 0.7 V. Thus, the bi-cell can work in a degraded mode under a lower operating voltage 0.7 V.

4.5. Net power of the bi-cell

The power consumption of the PZT device increases with increasing temperature due to the positive temperature-dependent dielectric constant of the PZT material [26]. Fig. 18 shows that the power consumption of the PZT device increases from 0.19 W to 0.26 W when operating temperatures increase from 30 °C to 60 °C. In this study, the optimal performance of the PZT-PEMFC-ND bi-cell is 0.91 W with an operating temperature of 50 °C, an anode flow rate of 60 ml min^{-1}, and a PZT vibration frequency of 60 Hz. Considering the power consumption of the PZT device, a maximum bi-cell net power of 0.7 W was obtained when T_{An} = 30 °C, T_{cell} = 40 °C, and f = 60 Hz. Thus, the temperature-dependant power consumption characteristics of the PZT device

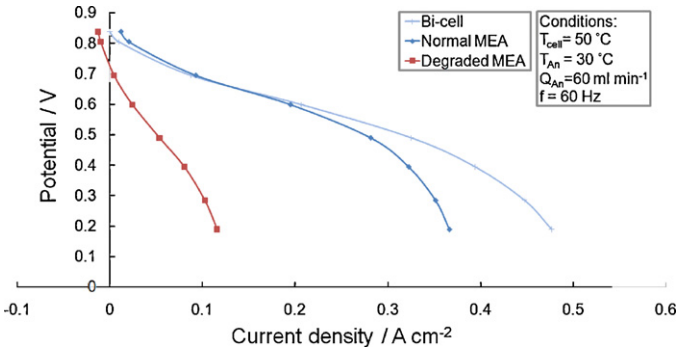

Fig. 17. The *I–V* curves of the bi-cell and the component cells at T_{cell} = 50 °C, T_{An} = 30 °C, Q_{An} = 60 ml min^{-1}, and f = 60 Hz.

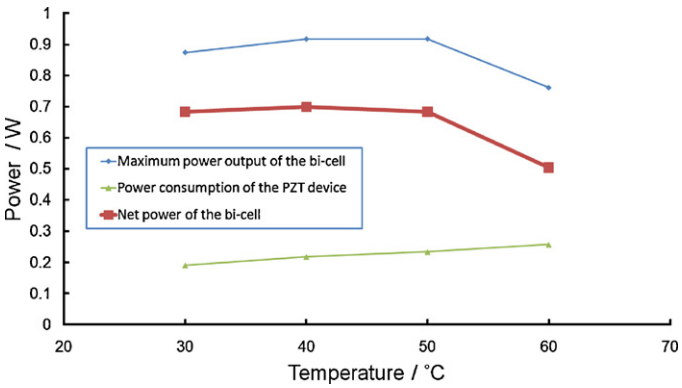

Fig. 18. The power consumption of the PZT device and the net power of the PZT-PEMFC-ND bi-cell under different temperatures.

should be taken into consideration when determining the net power of the PZT-PEMFC-ND bi-cell.

5. Conclusion

An innovative pseudo-bipolar design for the PZT-PEMFC-ND bi-cell, with a reduced nozzle and diffuser, has been successfully developed and its performance was investigated under different operating conditions as well as under a degraded working mode. The major findings are as follows:

(1) Cell temperature and stoichiometric ratio are the two most important operating parameters required to increase the performance of the PZT-PEMFC-ND bi-cell. Optimal bi-cell performance is obtained with a stoichiometric ratio of 1.5 and a cell temperature of 50 °C.
(2) PZT-PEMFC-ND pump performance may be influenced by the asymmetric amplitude of the PZT device. The asymmetric amplitude results in different air flow rates through the cathode chamber of the component cells and in different current outputs for the component cells.
(3) A stoichiometric ratio smaller than 1.5 may result in a concentration loss for the bi-cell and one component cell would suffer a serious concentration loss.
(4) The degraded MEA would result in a lower open-circuit voltage and an internal current inside the bi-cell. However the novel bi-cell can still deliver a non-negative power. In this study, the degraded MEA contributes to the performance of the bi-cell at an operating voltage lower than 0.7 V. This finding will enable the use of PZT-PEMFC-ND bi-cells in future stack designs.
(5) The power consumption of the PZT device is temperature-dependant and should be taken into consideration when determining the net power of the PZT-PEMFC-ND bi-cell. In this study, the maximum net power of the bi-cell was found to be 0.7 W.

Acknowledgement

This research was funded by the National Science Council of the Republic of China (NSC 99-2221-E-002-126-MY2 and NSC 99-2622-E-002-029-CC3).

References

[1] P. Costamagna, S. Srinivasan, J. Power Sources 102 (2001) 242–252.
[2] P. Costamagna, S. Srinivasan, J. Power Sources 102 (2001) 253–269.
[3] R. von Helmolt, U. Eberle, J. Power Sources 165 (2007) 833–843.
[4] X. Yang, Z. Zhou, H. Cho, X. Luo, Sens. Actuators A 130–131 (2006) 531–536.
[5] A. Olsson, G. Stemme, E. Stemme, Sens. Actuators A 47 (1995) 549–556.
[6] A. Ullmann, Sens. Actuators A 69 (1998) 97–105.

[7] K.S. Yang, I.Y. Chen, C.C. Wang, Chem. Eng. Technol. 29 (2006) 703–710.
[8] Q. Yan, H. Toghiani, J. Wu, J. Power Sources 158 (2006) 316–325.
[9] J.H. Jang, H.C. Chiu, W.M. Yan, W.L. Sun, J. Power Sources 180 (2008) 476–483.
[10] J.S. Yi, T.V. Nguyen, J. Electrochem. Soc. 145 (1998) 1149–1159.
[11] S. Ge, C.Y. Wang, J. Electrochem. Soc. 154 (2007) B998–B1005.
[12] D. Yu, S. Yuvarajan, J. Power Sources 142 (2005) 238–242.
[13] S. Lazarou, E. Pyrgioti, A.T. Alexandridis, J. Power Sources 190 (2009) 380–386.
[14] U. Reggiani, L. Sandrolini, G.L. Giuliattini Burbui, J. Power Sources 165 (2007) 224–231.
[15] R.P. Ramasamy, E.C. Kumbur, M.M. Mench, W. Liu, D. Moore, M. Murthy, Int. J. Hydrogen Energy 33 (2008) 3351–3367.
[16] Y. Zhang, R. Pitchumani, Int. J. Heat Mass Tran. 50 (2007) 4698–4712.
[17] W. Schmittinger, A. Vahidi, J. Power Sources 180 (2008) 1–14.
[18] H.K. Ma, S.H. Huang, B.R. Chen, L.W. Cheng, J. Power Sources 180 (2008) 402–409.
[19] H.K. Ma, S.H. Huang, Y.Z. Kuo, J. Power Sources 185 (2008) 1154–1161.
[20] H.K. Ma, S.H. Huang, J. Fuel Cell Sci. Technol. 6 (2009) 034501–34511.
[21] H.K. Ma, S.H. Huang, J.S. Wang, C.G. Hou, C.C. Yu, B.R. Chen, J. Power Sources 195 (2010) 1393–1400.
[22] H.K. Ma, J.S. Wang, Y.T. Chang, J. Power Sources 196 (2011) 3766–3772.
[23] R. Jiang, D. Chu, J. Power Sources 93 (2001) 25–31.
[24] Z. Xie, S. Holdcroft, J. Electroanal. Chem. 568 (2004) 247–260.
[25] D. Chu, R. Jiang, J. Power Sources 83 (1999) 128–133.
[26] D. Apte, R. Ganguli, CMC 10 (2009) 139–161.